On Methods for Low Velocity Friction Compensation: Theory and Experimental Study

John Adams — *Graduate Student*

Shahram Payandeh — *Assistant Professor*

Experimental Robotics Lab (ERL)

School of Engineering Science

Simon Fraser University

Burnaby, B.C.

Canada

V5A 1S6

Abstract

A study of different classes of controllers for mechanisms under the influence of low velocity friction is conducted. Many methods are proposed in the literature for friction compensation, but there has been no significant analysis of these methods with respect to each other. Also lacking in the literature is some form of categorization, under which it is possible to describe and study their performance. This paper provides an experimental and analytic study of controllers previously proposed for low velocity friction compensation. Since each controller will be evaluated on the same experimental platform, the results can be quantified to provide an approach by which to evaluate the performance of the controllers relative to each other. Some simulations will also be performed to show the effect of certain system parameters on the performance of these controllers.

1 Introduction

Friction within mechanisms is unavoidable. Rigid bodies in contact and moving relative to each other experience the effect of friction. The friction characteristic of rigid bodies moving relative to each other at substantial speed is fairly linear. As the velocity of the contacting bodies decreases, the frictional effects the mechanism experiences become highly nonlinear, and is not well understood. When the bodies in contact are at rest, there is an opposing frictional force equal to the applied force on the bodies. This sticking force (stiction, Fig. 1) will prevent any motion until the applied force can surmount the maximum stiction level inherent between the materials in contact. Thus at zero velocity it can be stated that the function is discontinuous, and is normally modelled by a signum function.

It has been experimentally determined [1], that immediately after motion has occured the friction decreases in value rapidly (reffered to as the *Stribeck effect*), to some lower level after which it will increase fairly linearly with velocity as shown in Fig. (1). For the different regions of the friction model, this paper will use the following notation:

τ_{stk}: The value of the stiction torque.

τ_{slp_0}: The lower bound on the downward bend.

τ_{slp}: Viscous friction.

Low velocity friction is sometimes called "Stick-Slip" friction. Stick-Slip friction puts a lower bound on the performance that can be extracted from a mechanism, such as minimum velocity achievable and persistent steady state errors. Symptoms of this phenomena in mechanisms attempting to move at low velocities can be anything from jerky motion or limit cycles, to catastrophic instability. The effects of Coulomb friction and Stiction have

influenced the design of many mechanisms, from the milling process [2], to applications involving space dynamics [3].

The factors affecting the frictional relationship between any two materials are very complex [4] [5]; among them are the normal force on the bodies, the length of time at which they have been at rest, the relative velocity, and some researchers have pointed out that even the history of velocity is also a determining factor. As such, the task of modelling the friction characteristics between bodies moving relative to each other is a challenging one.

For the analytical studies of this paper, a model of friction was chosen to be to be that of fig. (1). This model can be described mathematically as:

$$\tau_f = \tau_{slp}(\dot{q}) \cdot (\lambda(\dot{q})) + \tau_{stk}(\dot{q}) \cdot (1 - \lambda(\dot{q})) \tag{1}$$

where

$$\lambda(\dot{q}) \quad = \quad \begin{cases} 1 & \dot{q} > \alpha \\ 0 & \dot{q} \leq \alpha \end{cases}$$

α is the zero bound assigned to the velocity to facilitate numeric simulation [6], where any velocity within α is taken as zero. τ_{slp} is the function describing the friction at nonzero velocities, while τ_{stk} describes the friction when the velocity is zero (within α).

There are many models used to describe stiction and viscous friction. Stiction and viscous friction will be described mathematically as:

$$\tau_{stk} = \begin{cases} \tau & \tau \leq \tau_{stk} \\ \\ \tau_{stk} & \tau > \tau_{stk} \end{cases} \quad (2)$$

$$\tau_{slp} = sgn(\dot{q})(\tau_{stk} + [\tau_{slp_0} - \tau_{stk}][1 - \exp^{-a\dot{q}}]) + b\dot{q} \quad (3)$$

which is a nonlinear function, discontinuous at zero velocity, falling off exponentially to some lower bound τ_{slp_0}, then increasing linearly with nonzero velocity. b is the *damping coefficient*, the rate at which the viscous friction increases with respect to velocity; τ is the applied torque to the system. The signum function is modelled mathematically as:

$$sgn(\dot{q}) = \begin{cases} 1 & \dot{q} > 0 \\ \\ 0 & \dot{q} = 0 \\ \\ -1 & \dot{q} < 0 \end{cases}$$

This paper will examine controller classes proposed for the purpose of compensating for stick slip friction in mechanisms undergoing free motion. Compensation categories will be divided into linear and nonlinear. The linear control schemes consist of PD and PID methods. The nonlinear class will consider nonlinear compensators which supplement the existing linear controllers. Section (2) will describe the system used to test these compensators, as well as provide the set of equations of motion that govern it. Sections (3) and (4) provide a theoretical analysis of the linear and nonlinear controllers respectively. In section (5) the experimental setup will be described as well as a discussion of the results obtained from

implementing each of the controllers in the previous sections. Concluding remarks on the nature of these compensation schemes are presented in section (6).

2 System Description

The experimental platform is a 2 DOF planar manipulator, with known dynamics. For our experiments and simulations, unconstrained motion of the distal link is considered (Fig. 6), in effect creating a 1 DOF system with no gravitational effects. The complete system equation for the 2 DOF manipulator are formulated as:

$$I(q)\ddot{q} + C(q,\dot{q})\dot{q} = \tau - \tau_f \tag{4}$$

with $I(q)$ being the system inertial matrix, and $C(q,\dot{q})$ the matrix of coriolis and centrifugal terms. where:

$$I(q) = \begin{bmatrix} p_1 + 2p_3 cos(q_2) & p_2 + p_3 cos(q_2) \\ p_2 + p_3 cos(q_2) & p_2 \end{bmatrix}; \qquad C(q,\dot{q}) = \begin{bmatrix} -\dot{q}(2\dot{q}_1 + \dot{q}_2)p_3 sin(q_2) \\ \dot{q}_1^2 p_3 sin(q_2) \end{bmatrix} \tag{5}$$

The terms p_1 to p_3 are constants defined by the dynamics of the system. q_1 and q_2 are the angular position of the proximal and distal joints respectively.

For the 1 DOF system, we assume q_1 and all its derivatives are zero. Thus the equation of motion can be written as:

$$p_2\ddot{q}_2 = \tau_2 - \tau_f \tag{6}$$

where p_2 consists of the elbow link inertia and also the motor rotor inertia. For the rest of the paper, p_2 will be considered to be the inertia of the system and denoted I, τ_2 to be the applied torque τ, and q_2 as the joint variable q. We thus have a set of scalar equations which describe the dynamics of the system:

$$I\ddot{q} = \tau - \tau_f \tag{7}$$

τ_f is the disturbance due to friction, nonlinear in general.

3 Linear Methods

3.1 PD schemes

Proportional plus derivative is a linear time-invariant method of joint control in manipulators. It has also been shown to be globally asymptotically stable [7].

The main drawback of PD control when the system dynamics include dry friction, is the existence of a steady state error throughout the trajectory. It is well known that increasing the proportional gain can reduce these errors, but the required accuracy may well be beyond the capacity of the actuators, and increasing proportional control also results in increased oscillatory behavior. For example, given a set of controller gains, when the angle of the distal link is within the proximity of the reference, the position error is small, thus the resulting proportional gain is unable to surmount the stiction level in the joint. Hence the control

torque is unable to overcome the opposing friction force.

For the system described in (7), the closed loop dynamics with a PD controller become:

$$\tau = -k_p(q) - k_d(\dot{q}) \tag{8}$$

$$\ddot{q} = -\frac{1}{I}(k_p(q) + k_d(\dot{q}) - \tau_f) \tag{9}$$

It has been shown by Hahn [8] using a mass-spring model, that the discontinuity associated with dry friction when proportional control is present, will cause multiple stable equilibrium points. These equilibrium points occur when trajectories at zero velocity, are within certain limits of the position error, and any trajectory within these limits at zero velocity will get stuck.

The system was simulated to show the existence of these equilibria. The friction model of eq.(1) is used for this simulation. The plots (Fig. 3) show the convergence for the system with and without dry friction. For a given set of parameters, the reference point was set further and further away from the origin. The parameters used in this simulation were:

$$\begin{aligned} k_p &= 50 \\ k_d &= 4 \\ \tau_{stk} &= 2\ N.m \\ \tau_{slp_0} &= 1\ N.m \\ b &= 1\ N.m/rad.sec^{-1} \\ I &= 1\ Kg.m^2 \end{aligned} \tag{10}$$

The trajectories terminated within the bounds as specified in [8].

3.2 PID Control

PID control is another linear time-invariant method for joint control, and is one of the more popular industrial approaches. The advantage of PID control is that it leaves no steady state error ($e_{ss} \rightarrow 0 \; as \; t \rightarrow \infty$). Cancelation of the steady state error is due to the presence of integral control action which has been shown to be robust [9].

Substituting the PID control law into the system open loop dynamics (eq. (7)), The system dynamics become:

$$\ddot{q} = -\frac{1}{I}(k_p(q) + k_d(\dot{q}) + k_i \int_{t_0}^{t} q \cdot dt - \tau_f) \tag{11}$$

Integral action in a control law with dry friction present has been shown to be capable of producing limit cycles. A limit cycle is a periodic equilibrium point. They are characterized by trajectories circling the origin at a constant radius in the state-plane. Both describing function analysis [10] and the contraction mapping theorem [11] [12], have been used to show its existence.

A system under PID control can be made unstable when the moving body (joint of the manipulator) is stuck and the control gains are too high. As time proceeds, the integral error which is building up to move the joint from its stuck configuration becomes so high that the joint overshoots the origin and comes to rest further away from it. This will cause a larger integral action, and the effect is cascaded. This is demonstrated by taking the system described by (11) and running the simulation with a large integral gain and initial conditions

which place the system inside a sticking region.

Numeric simulations are performed to show the effect various changes in the system dynamics can have on the trajectory, and reveal contraction mappings for the system described in 11. When a set mapped onto itself is a contraction mapping, then there is a unique fixed solution (in other words, a limit cycle) for that mapping within the set [12]. However it remains to show that the mapping of the set of points within a sticking portion of the trajectory back onto itself is indeed a contraction mapping. Theoretical methods used to show this [12] [13], rely on the mapping function to satisfy a Lipschitz condition. With Coulomb friction in the system dynamics, this is not the case, so the use of numeric simulations must be used instead [11].

Figure (4) shows trajectory behaviors and indicate the existence of limit cycles for the friction model described in eq.(1). Figure (4a) shows the trajectory for the default parameters of the friction model (eq.(10) and an integral gain of Ki = 100). In Fig.(4b) the proportional gain is doubled, as expected the amplitude of the limit cycle is halved. This is consistent with the fact that twice the proportional gain will cause the actuators to output twice the amount of torque for a given position error. Fig.(4c) shows the trajectory when the integral gain is increased by a factory of 5; the spiral is a source and extends outwards indicating an unstable system. The damping coefficient was then increased by a factory of 5 shown in Fig.(4d), the limit cycle amplitude remained constant as the system is dampened.

To further examine the response, one of the trajectories used to test the response of the PD controller was used with the PID controller to see the difference. A step input was applied to the system, and its convergence properties were studied in the state space. The limit cycle persisted with the PID scheme, but its amplitude was much less than the steady

state error exhibited by the PD controller for the same step input (Fig.(4e))

4 Nonlinear Methods

This section presents an analytic overview of two nonlinear controllers presented in the literature, [14] [15]. Both controllers use a nonlinear feedforward compensation scheme to supplement a PD control law. The methods differ with respect in which the compensating controller is implemented. In [15], a piecewise linear function is generated which is a function of the sticking limits similar to those shown in [8], (e.g. Fig(3(a)). The other nonlinear compensator implements a tanh() function which is continuous and twice differentiable. Bounded stability of both controllers is demonstrated. Lyapunov's direct method is used in [14], whereas a modified version of Lyapunov's direct method employing the notion of the dini-derivative is used in [15] to account for the fact that the controller is discontinuous at the origin. In [14], Lassalle's theorem is exploited to show asymptotic convergence of the solution trajectories, as well as error bounds within which the trajectories will converge.

In the sections to follow, an analytic overview of these methods will be presented, with proofs of their stability.

4.1 Smooth Continuous Nonlinear Compensation

The control law in [14] uses a nonlinear addendum to supplement an existing PD scheme. The feedforward additive is a $tanh()$ function of setpoint error. This forces an extra input to be fedforward until the error is within the proximity of zero, the accuracy of which is controlled by a parameter in the $tanh()$ function.

The proposed control law is defined as:

$$\tau = -k_p q - k_d \dot{q} - \tau_c(q) \tag{12}$$

$$q = position\ error.$$

$$\tau_c(q) = \tau_{mstk} \tanh(\alpha q) \tag{13}$$

$$\tau_{mstk} = \tau_{stk} + \epsilon \tag{14}$$

$$\tau_{stk} = maximum\ stiction\ torque$$

The maximum stiction torque can be experimentally determined, then supplemented by a small positive constant ϵ to guarantee the stiction levels are always exceeded. The unitless constant α (not to be confused with that used in the friction model (1)).is used to adjust the slope of the $tanh()$ function in the vicinity near zero error. This in turn adjusts the steady state error achievable. This controller is illustrated in Fig. 5. To get an estimate of the value to use for α, the function $\tanh(\alpha x)$ can be plotted for x values around the vicinity of the maximum tolerable error. α can be changed till the function saturates at an x value within the specified error tolerance.

The controller adds an extra compensating torque equal to the magnitude of τ_{mstk}, which always exceeds the magnitude of the sticking torque of the joint. This forces the trajectory to a unique equilibrium point closer to the origin.

Using our 1DOF system equation (7), and control law described by (12), we get the system's equation:

$$I\ddot{q} = -k_d\dot{q} - k_p q - \tau_c(q) + \tau_f \tag{15}$$

The friction model used is similar in form to eq.(1), with τ_{stk} defined as in (2). To investigate the robustness character of the controller, different models are used for defining τ_{slp}, one of which is (3), and is formulated as:

$$\tau_f = -sgn(\dot{q})\tau_{slp} - (1 - \|sgn(\dot{q})\|)\tau_{stk} \tag{16}$$

The system (15), is globally asymptotically stable with the nonlinear term given by (13). To show this, a Lyapunov function candidate is selected as follows:

$$V = \frac{1}{2}I\dot{q}^2 + \frac{1}{2}k_p q^2 + \frac{\tau_{stk}}{\alpha}\ln(\frac{e^{\alpha q} + e^{-\alpha q}}{2}) \tag{17}$$

which is positive definite and satisfies a Lipschitz condition. Its derivative, by substituting the system dynamics (15) into (17) can be written as:

$$\begin{aligned}
\dot{V} &= I\dot{q}\ddot{q} + \frac{1}{2}\dot{I}\dot{q}^2 + k_p q\dot{q} + \tau_{stk}\tanh(\alpha q)\dot{q} && (18)\\
&= -k_d\dot{q}^2 + \dot{q}\tau_f && (19)\\
&= -k_d\dot{q}^2 - \dot{q}\cdot sgn(\dot{q})\tau_{slp} - (1 - \|sgn(\dot{q})\|)\tau_{stk} && (20)\\
&= -k_d\dot{q}^2 - \|\dot{q}\|\tau_{slp} \leq 0 && (21)
\end{aligned}$$

For a 1DOF system, there are no coriolis terms, and the inertial component of the

dynamics is time invariant ($\dot{I} = 0$). Equation (21) and inequality arises from the definition of τ_f, and the fact that for any q, there exists the relationship $q \cdot sgn(q) \geq 0$. $\dot{\mathrm{V}} = 0$ only when $\dot{\mathrm{q}} = 0$; so by Lassalle's theorem the system is globally asymptotically stable [16]. The concept of the invariant set used with Lassalle's theorem is used again to reveal the bounds on the error. It is known that the steady state solution of $\dot{V}$ will converge to a value within the largest invariant set, thus the invariant set will provide the bounds on the steady state error.

Let E be the invariant set, and substitute the conditions therein into the system dynamics, and using the inequality $\tau_{stk} \leq \tau_{mstk}$, we get:

$$\begin{aligned} E &= \{q \in R |\ \ddot{q} = \dot{q} = 0\} \\ &= \{q \in R |\ k_p \|q\| + \tau_{mstk} \tanh(\alpha \|q\|) \leq \tau_{stk}\} \end{aligned} \tag{22}$$

The two arguments on the left of the inequality in (22) are always greater than or equal to 0, then we have:

$$\tau_{mstk} \tanh(\alpha \|q\|) \leq \tau_{stk} \tag{23}$$

solving (23) we can have the following bound on q inside the invariant set, indicating the bounds on the steady state error:

$$q \leq \frac{1}{2\alpha} \ln(1 + 2 \cdot \frac{\tau_{mstk}}{\alpha}) \tag{24}$$

4.2 Discontinuous Compensation

This controller uses the sticking limits q_h and q_l given in in Fig. 6, to provide bounds within which extra compensating torque will be applied [15]. Unlike the previous method, this compensating input is only applied when the position error is small enough to bring about sticking (see fig. 6). The added input ceases when the position error is zero.

The friction model used to demonstrate this controller is the same as that defined in eq's. (1) to (2). τ_{slp} is assumed to be an arbitrary continuous function satisfying a Lipschitz condition.

The control law is defined as follows:

$$\tau = -k_p q - k_d \dot{q} - \tau_c(q) \tag{25}$$

$$\tau_c(q) = k_p q_c = compensating\ control$$

$$q_c = \begin{cases} 0 & q > q_h \\ (q_h - q) & 0 < q \leq q_h \\ 0 & q = 0 \\ (q_l - q) & q_l \leq q < 0 \\ 0 & q < q_l \end{cases} \tag{26}$$

Stability is proven using a modified version of Lyapunov's direct method, involving the notion of the "Dini-Derivative" for the discontinuous trajectories in the controller. The energy function is similar to that used in [14] except for the nonlinear addendum. The Lyapunov function candidate is formulated as follows:

$$V = \frac{1}{2} I \dot{q}^2 + \frac{1}{2} k_p q^2 + g(q) \tag{27}$$

where,

$$g(q) = \begin{cases} \frac{1}{2} k_p (q_h)^2 & q > q_h \\ k_p (q_h q - \frac{1}{2} q^2) & 0 \leq q \leq q_h \\ k_p (q_l q - \frac{1}{2} q^2) & q_l \leq q \leq 0 \\ \frac{1}{2} k_p (q_l)^2 & q < q_l \end{cases} \tag{28}$$

This nonlinear addendum is shown graphically in fig(7).

It can be seen from (27) and Fig(7) that this energy function is positive definite as well as decrescent for trajectories outside the region of discontinuity. Using the 1DOF dynamic model of the distal link defined in eq.(7)and the controller of eq.(25), the derivative of the energy function of eq.(27) along the solution trajectory can be written as:

$$\dot{V} = k_p q \dot{q} + I \dot{q} \ddot{q} + \dot{g}(q) \dot{q} \tag{29}$$

$$= k_p q \dot{q} + \dot{q}(\tau - \tau_f) + \dot{g}(q) \dot{q} \tag{30}$$

which from eqs.(1) - (2), (25), and the fact that outside the discontinuity τ_{stk} is zero, can be written as:

$$\dot{V} = -k_d \dot{q}^2 - \dot{q}\ \tau_{slp}(\dot{q}) + \dot{q}(\dot{g}(q) - k_p q_c) \tag{31}$$

From eq.(26) and eq.(28) we see that $k_p q_c = \dot{g}(q)$ except when $q = 0$, where $\dot{g}(q)$ is undefined. eq.(31) becomes:

$$\dot{V} = -k_d \dot{q}^2 - \dot{q}\tau_{slp}(\dot{q}) \leq 0 \tag{32}$$

For the trajectories within the region of discontinuity, the notion of the 'Dini-Derivative' is used. These are the limiting values of $\dot{V}$ on both sides of the discontinuous region, and denoted $D * \dot{V}(\cdot)$, and can have any of four values. For any point on the trajectory where $\dot{V}$ exists, the four possible dini-derivatives have a common value equal to that of the regular derivative [17]. Since V is continuous, and $\dot{V}$ is negative semi definite (n.s.d.) outside of the discontinuous region, the dini-derivatives are also n.s.d. for points within the region. The dini-derivatives are therefore n.s.d. over the entire trajectory, and from eq.(32), $\dot{V} = 0$ implies $\dot{q}$=0 which is the q axis, and no complete trajectories can be contained there, so $D * \dot{V}(\cdot)$ is negative definite over the entire trajectory, implying global asymptotic stability.

5 Experimental Results

5.1 Experimental Setup

Each controllers which have been discussed in the previous sections has been implemented on a planar 2DOF manipulator, with the base link held stationary while the elbow followed a trajectory.

The test trajectory for the joint is a 90^o clockwise rotation following a smooth (inverted cosine curve) velocity profile. A smooth acceleration profile commencing at 0 (sine curve)

was chosen so as not to cause extreme setpoint error at the start and end of motion. The entire trajectory has been parameterized as follows:

$$\begin{aligned} accn &= amax \cdot \sin(\frac{2\pi t}{T}) \\ vel &= -amax \cdot \frac{T}{2\pi} \cdot \cos(\frac{2\pi t}{T}) + amax \cdot \frac{T}{2\pi} \\ dist &= -amax \cdot (\frac{T}{2\pi})^2 \cdot \sin(\frac{2\pi t}{T}) + amax \cdot \frac{T}{2\pi} \cdot t \end{aligned}$$

To further parameterize this profile, the maximum velocity and rotation angle is specified as:

$$\begin{aligned} amax &= \frac{\pi \cdot vmax}{T} = \frac{2\pi \cdot dist}{T^2} \\ T &= \frac{2 \cdot dist}{vmax} \\ amax &= \frac{\pi \cdot vmax^2}{2 \cdot dist} \end{aligned}$$

where we have defined:

$accn$: angular acceleration,

vel : angular velocity,

$dist$: degrees to rotate,

$amax$: maximum acceleration,

$vmax$: maximum velocity.

The manipulator uses brushless DC motors that have high torque capabilities. The motor responsible for the distal joint has a maximum torque output capability of 39 N.m, and has

a resolver that gives 153,600 counts per revolution. This is read by a quad decoder on a data acquisition card using a PC as the workstation. The control algorithm was executed at a sample rate of 1 msec. and is run on a DSP processor, to which the data acquisition board is connected.

The data sampled consists of link position, output torque, and commanded position, from which are calculated the actual velocity, commanded velocity, and positioning error.

The stiction level of the joint was found experimentally by applying a linearly increasing torque to the joint motor, till motion is detected. This was found to be around 2N, and ϵ used for the smooth nonlinear controller (eq.(14)) is taken as 0.5 N.m. With this data, the experiment was conducted implementing each of the controllers.

5.2 Results and Discussion

In comparison with the PD controller (Fig.8-9), it is apparent that both nonlinear controllers (Fig. 12, 13), and the PID scheme (Fig. 10-11) offer superior performance.

As demonstrated in the simulations, the amplitudes of the limit cycles associated with the PID controller are well below the steady state error level of a PD controller even when the proportional gain is increased.

The velocity lag at the beginning of motion is seen with the PD and PID controllers (Fig.(8) - (11)). This is due to the inherent stiction level. Before any motion can commence, both the integral and proportional gains must be large enough to counteract this effect. The rate of increase of the integral control being proportional to time, and that of the proportional control increasing with position error.

The nonlinear controllers however don't exhibit this lag (Fig. (12) - (13)), and also offer better tracking performance. This is due to the nature of the nonlinear compensators. There is no latency period for the gains to build up to a level large enough to counteract the stiction; once the error is small enough, the additive compensation is activated and there is enough torque to overcome stiction. Once this initial lag is finished however, the tracking performance of PID controller is not much inferior to the two nonlinear controllers.

The drawback of the nonlinear controllers is with their oscillatory response and their jerky torque profiles. In effect, these nonlinear controllers are simply error dependent high proportional gain controllers; as a, result, whenever more control input is needed the proportional gain increases and so does the oscillations and erratic torque outputs. There is no additional damping added in either control law. A look at the torque profile for the controller in [14] in fig.(12) shows this. This controller adds extra stiction compensating torque at all points on the trajectory, not just when needed, as a result the effective proportional gain of the smooth nonlinear controller is always higher than that of the discontinuous one, and the linear controllers.

A comparison between Fig's. (12) and (13) will show that the controller in [15] has much less oscillations at the end of its trajectory than does the controller in [14]. The oscillations at the beginning of motion are due to the fact that when the nonlinear compensation is dominant, which is due to a small setpoint error and stiction being in effect, there is a proportional control that acts with relatively little damping. Due to inertia effects, stiction is not present as the link approaches the reference point, and the motion at the end of the trajectory does not need the compensating control as at the beginning. The smooth controller however, has a high proportional gain approaching the end of the trajectory, and

as the error decreases, so does the derivative control, causing an underdamped oscillatory response. On the other hand, the discontinuous controller has a normal PD gain approaching the reference point and so does not to excite the system into oscillatory behavior.

From (24), it is obvious that the setpoint errors do not lie within the bounds predicted theoretically. The derivation of this bound was done using conditions of the invariant set that show this controller to be stable. The time constant of the theoretical system is much too large to be realized by any real system implementing setpoint control, i.e. a new setpoint will be generated long before the convergence time of the theoretical system; thus this error bound is not readily achievable in practice.

6 Conclusions

Classes of controllers for a manipulator joint under the influence of low velocity friction have been compared. Linear and nonlinear methods were used in the comparison. The linear methods consisted of PD and PID compensators, while the nonlinear compensators consisted of a piecewise linear compensation model as well as a smoother continuous model. The experiments were done on a 2DOF planar manipulator, using the distal link, in effect creating a 1DOF type manipulator. Both nonlinear controllers proved superior in performance to a PD controller for the same P and D gains, even when higher gains are used with the PD controller. Their tracking performance was also superior to the PID type controller, but at a cost of oscillatory response and jerky torque profiles. The two nonlinear controllers appear to give similar performance for tracking accuracy, however if the nature of motion is taken into account, the discontinuous controller has the advantage of providing much smoother motion

through a much less oscillatory response. This is due to the lower overall proportional control imposed on the system over the entire trajectory. The stability of the smooth controller is much simpler to demonstrate, as are the error bounds, which are shown however, not to be realizable with setpoint control.

The PID controller offers a good combination of tracking accuracy and smoothness of response, even with the limit cycles. It has also been shown that the small amplitude of these limit cycles does not have an adverse effect of the system behavior, while maintaining tracking accuracy, when unconstrained motion is considered.

References

[1] B. Armstrong, "Friction: Experimental determination, modelling and compensation," *Proc. of the 1988 Int'l. Conf. on Robotics and Automation*, pp. 1422–1427, 1988.

[2] J. H. Chin and C. C. Chen, "A study of stick slip motion and its influence on the cutting process," *International Journal of Mechanical Science*, vol. 35, no. 5, pp. 353–370, 1993.

[3] W. S. Newman, G. D. Glosser, J. H. Miller, and D. Rohn, "The effects of friction on space microgravity robots," *Proceedings of the IEEE Int. Conf. on Robotics and Automation*, vol. 2, pp. 1436–1441, 1992.

[4] J. Martins, J. Oden, and F. Simoes, "A study of static and kinetic friction," *International Journal of Engineering Science*, vol. 28, no. 1, pp. 29–92, 1990.

[5] S. W. Shaw, "On the dynamic response of a system with dry friction," *Journal of Sound and Vibration*, vol. 108, no. 2, pp. 305–325, 1986.

[6] D. Karnopp, "Computer simulation of stick slip friction in mechanical dynamical systems.," *Journal of Dynamic Systems, Measurement and Control*, pp. 100–103, March 1985.

[7] M. W. Spong and M. Vidyasagar, *Robot Dynamics and Control*. John Wiley and Sons, N.Y., 1989.

[8] W. Hahn, *Stability of Motion*. Springer-Verlag, 1967.

[9] S. Payandeh and A. Goldenburg, "A robust force controller: Theory and experiments," *Proc. of the I.E.E.E. Conf. on Robotics and Automation*, pp. 36–41, 1991.

[10] C. Canudas de Wit, P. Noel, A. Aubin, and B. Brogliado, "Adaptive friction compensation in robot manipulators: Low velocities," *Int'l Journal of Robotics Research*, vol. 10, no. 3, pp. 189–199, 1991.

[11] C. Radcliffe and S. Southward, "A property of stick-slip friction models which promotes limit cycle generation," *I.E.E.E. American Control Conference*, vol. 2, pp. 1198–1203, 1990.

[12] J. Holtzman, *Nonlinear System Theory: A functional Anlysis Approach*. Prentice-Hall, Inc., 1970.

[13] A. Kolmogorov and S. Fomin, *Functional Analysis*, vol. 1. Graylock Press ,Rochester, N.Y., 1957.

[14] L. Cai and G. Song, "A smooth robust nonlinear controller for robot manipulators with joint stick-slip friction," *Proc. of the I.E.E.E. Conf. on robotics and Automation*, pp. 449–454, 1993.

[15] C. Radcliffe, S. Southward, and C. MacCluer, "Robust nonlinear stick-slip friction compensation," *Journal of Dynamic Systems, Measurement, and Control*, vol. 113, pp. 639–644, December 1991.

[16] J. J. Craig, *Adaptive Control of Mechanical Manipulators.* Addison-Wesley, 1988.

[17] N. Rouche, P. Habets, and N. Laloy, *Stability Theory by Lyapunov's Direct Method.* Springer-Verlag, New York, 1977.

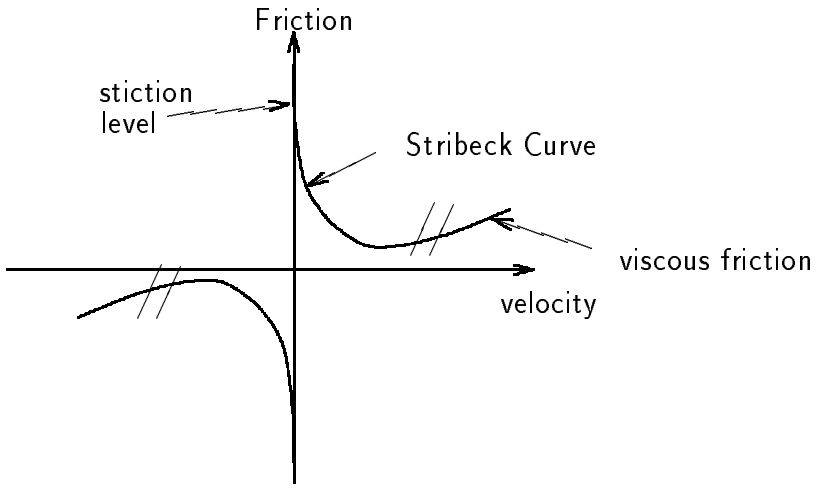

Figure 1: Friction/Velocity characteristic

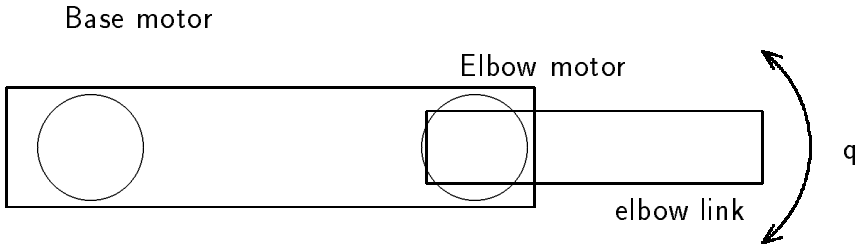

Plan view of 2 DOF scara type manipulator

Figure 2: Experimental platform used to test controllers

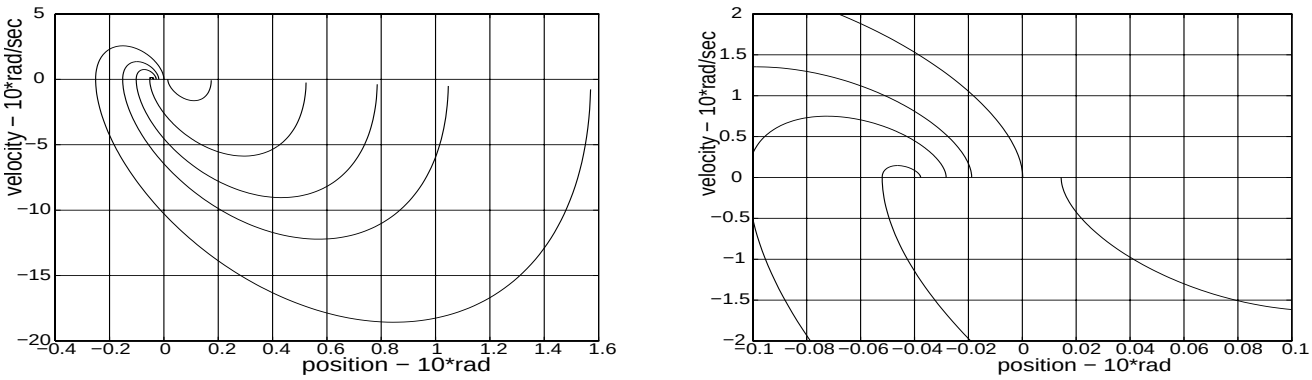

(a)

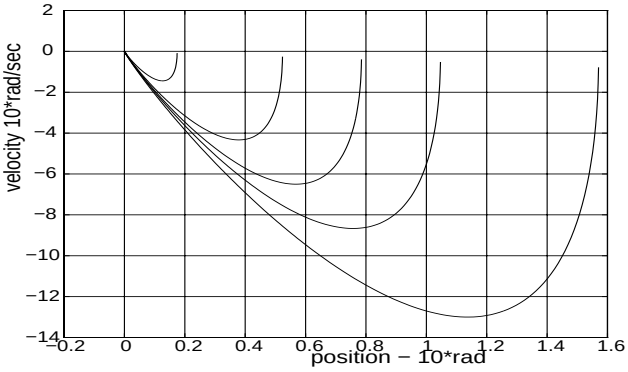

(b)

Figure 3: PD trajectories for 1DOF model both in the presence and absence of friction; Kp=100, Kd=4. The steady state errors with dry friction are bounded as described by Hahn. There is no steady state error present with the absence of dry friction. (a) Dry friction present, (b) No friction present.

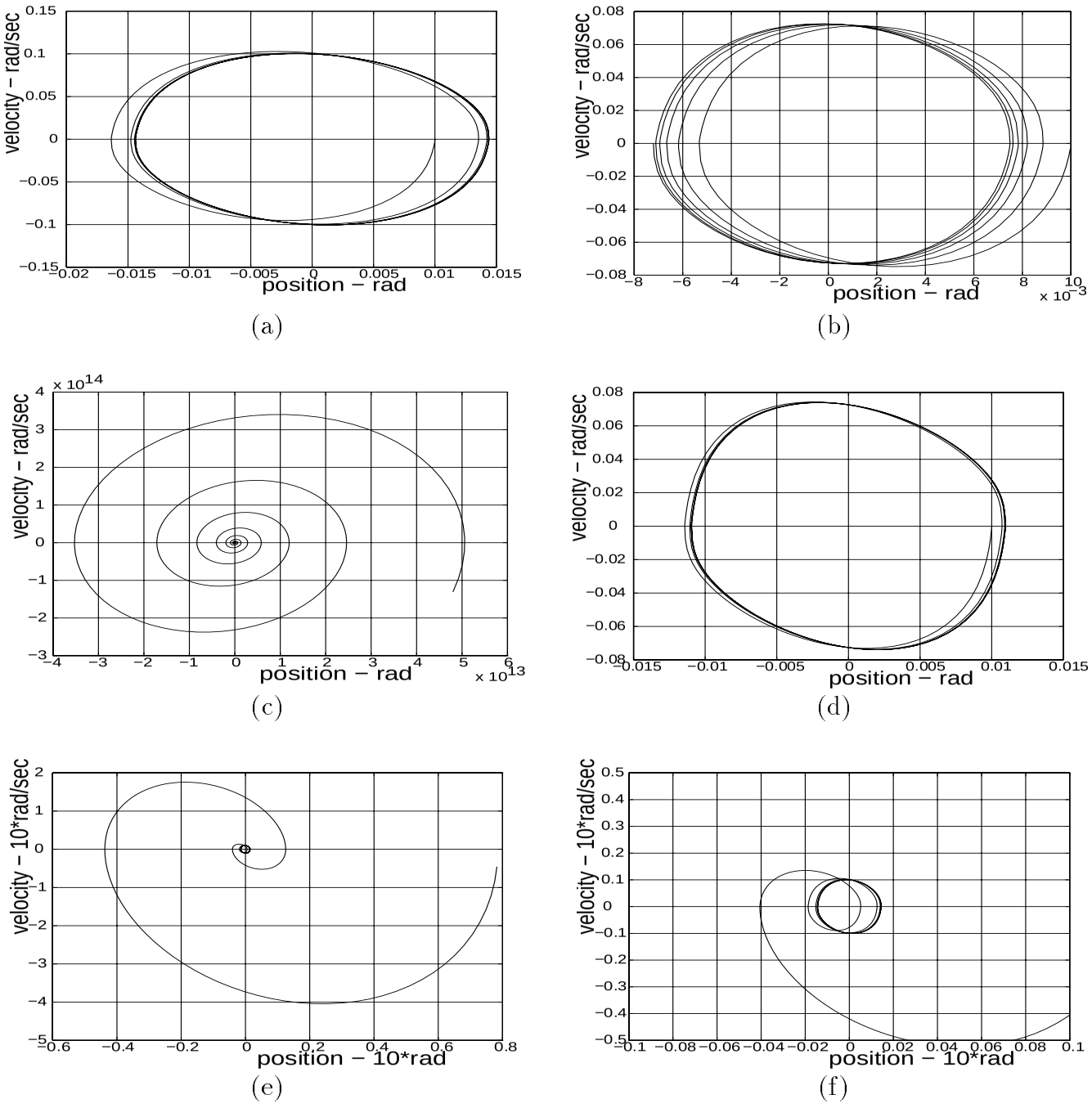

Figure 4: Simulation results of system with PID control showing limit cycles. (a) Default parameters Kp = 50, Kd = 4, Ki = 100; (b) Kp = 100; (c) Ki = 500; (d) b = 5; (e) System under PID control using an identical trajectory from PD simulations; (f) closeup of (e).

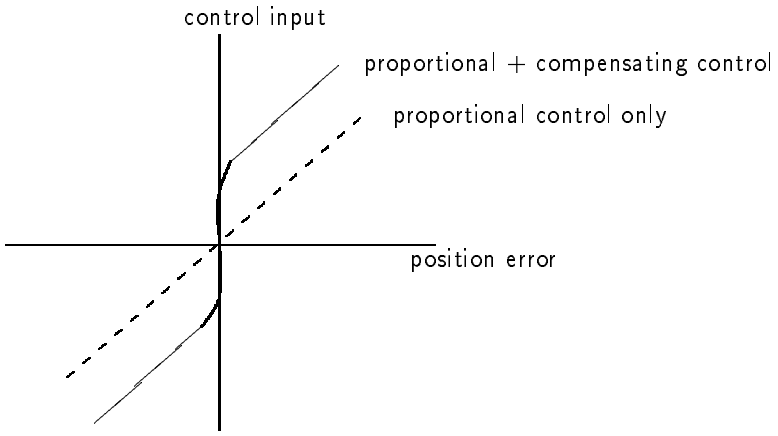

Figure 5: Smooth Nonlinear Controller

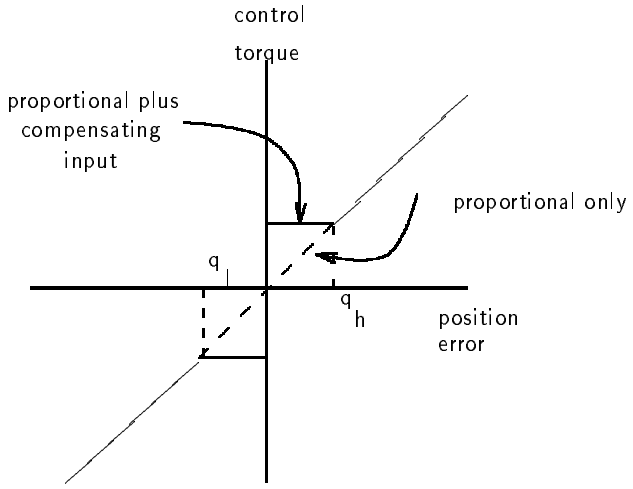

Figure 6: Piecewise linear controller

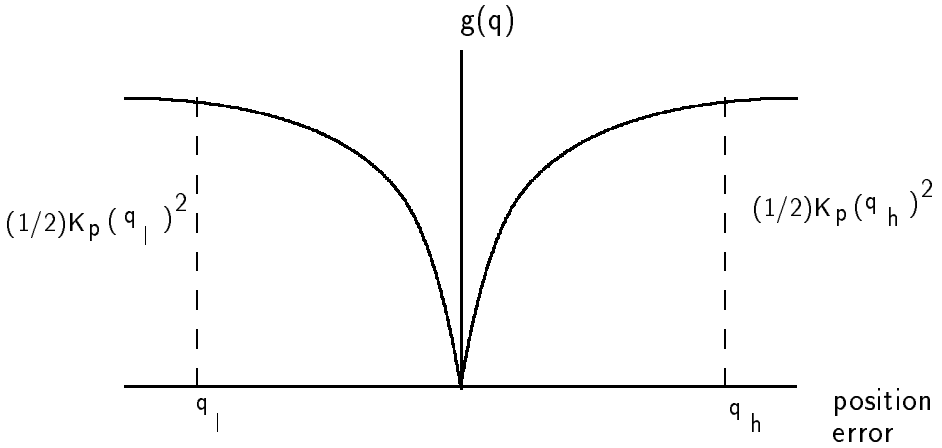

Figure 7: Nonlinear addition to Lyapunov energy function

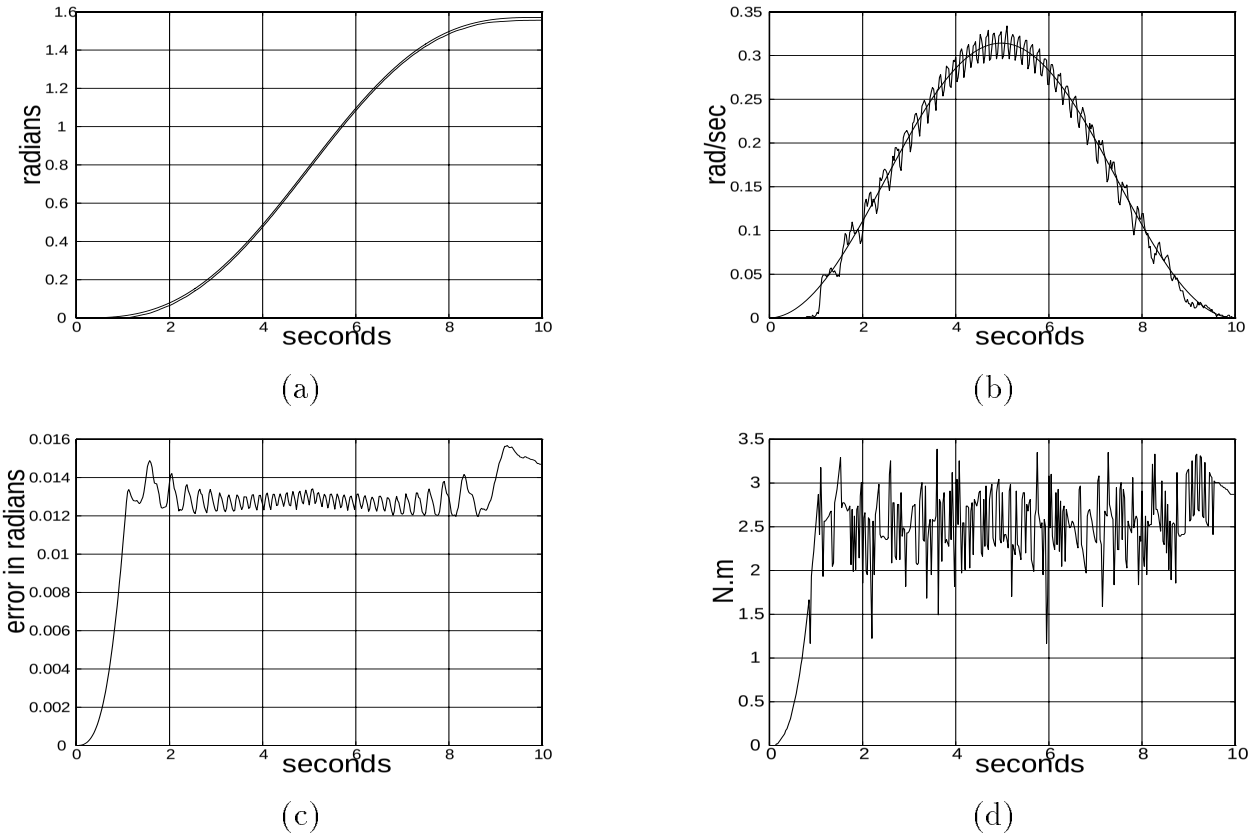

Figure 8: Experimental Results for the PD Controller. (a) Real and commanded position of elbow, (b) Real and commmanded velocity, (c) Tracking error, (d) torque profile

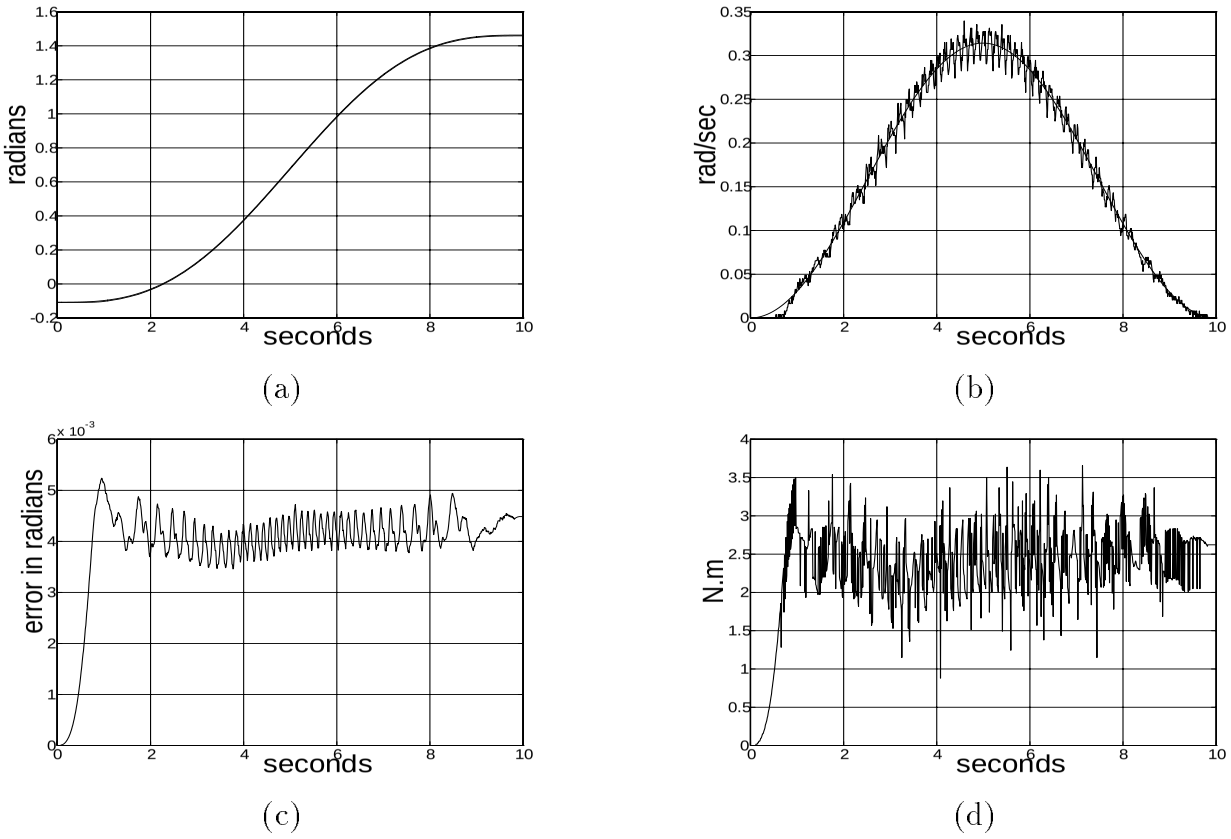

Figure 9: Experimental Results for the High Gain PD Controller. (a) Real and commanded position of elbow, (b) Real and commmanded velocity, (c) Tracking error, (d) torque profile

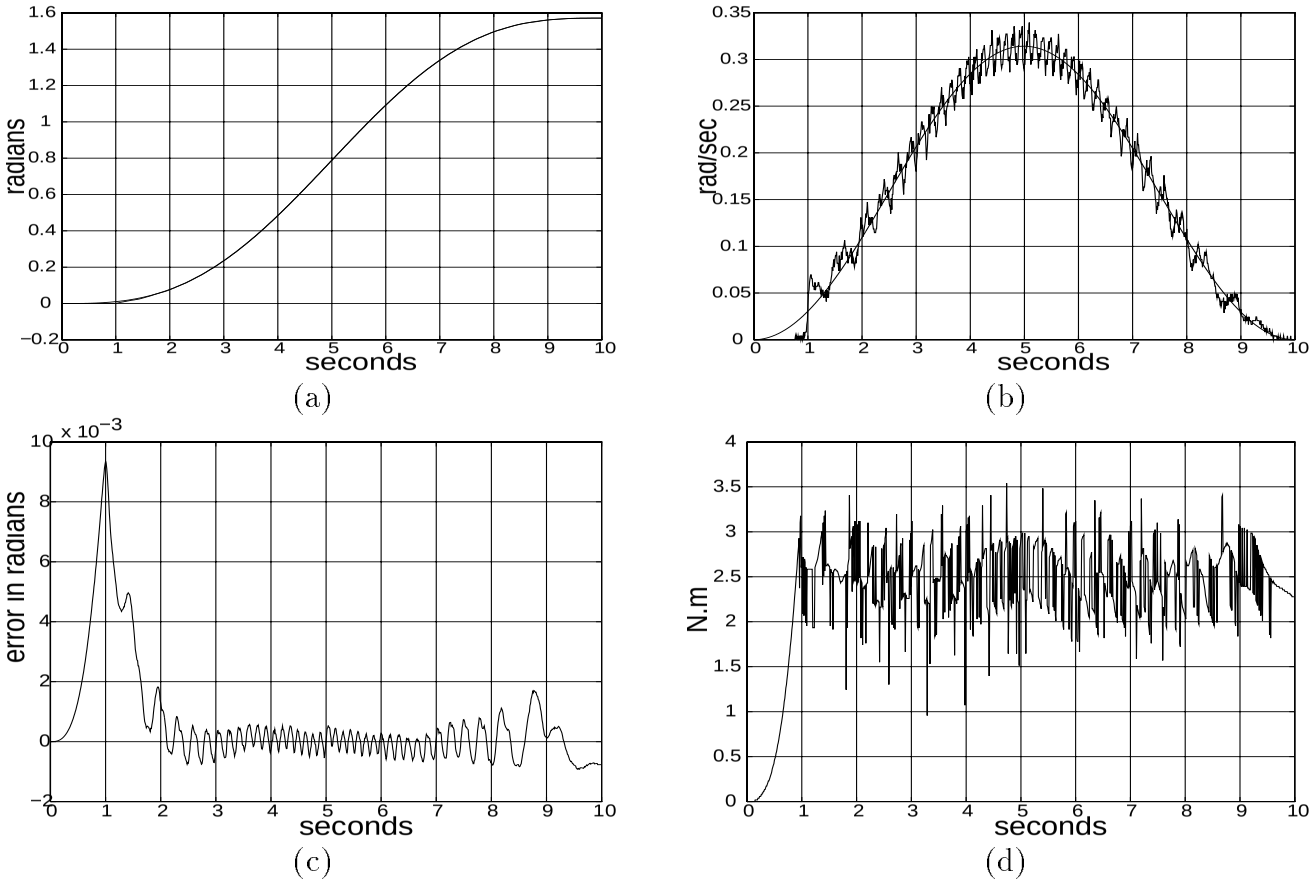

Figure 10: Experimental Results for the PID Controller, Ki=100. (a) Real and commanded position of elbow, (b) Real and commmanded velocity, (c) Tracking error, (d) torque profile

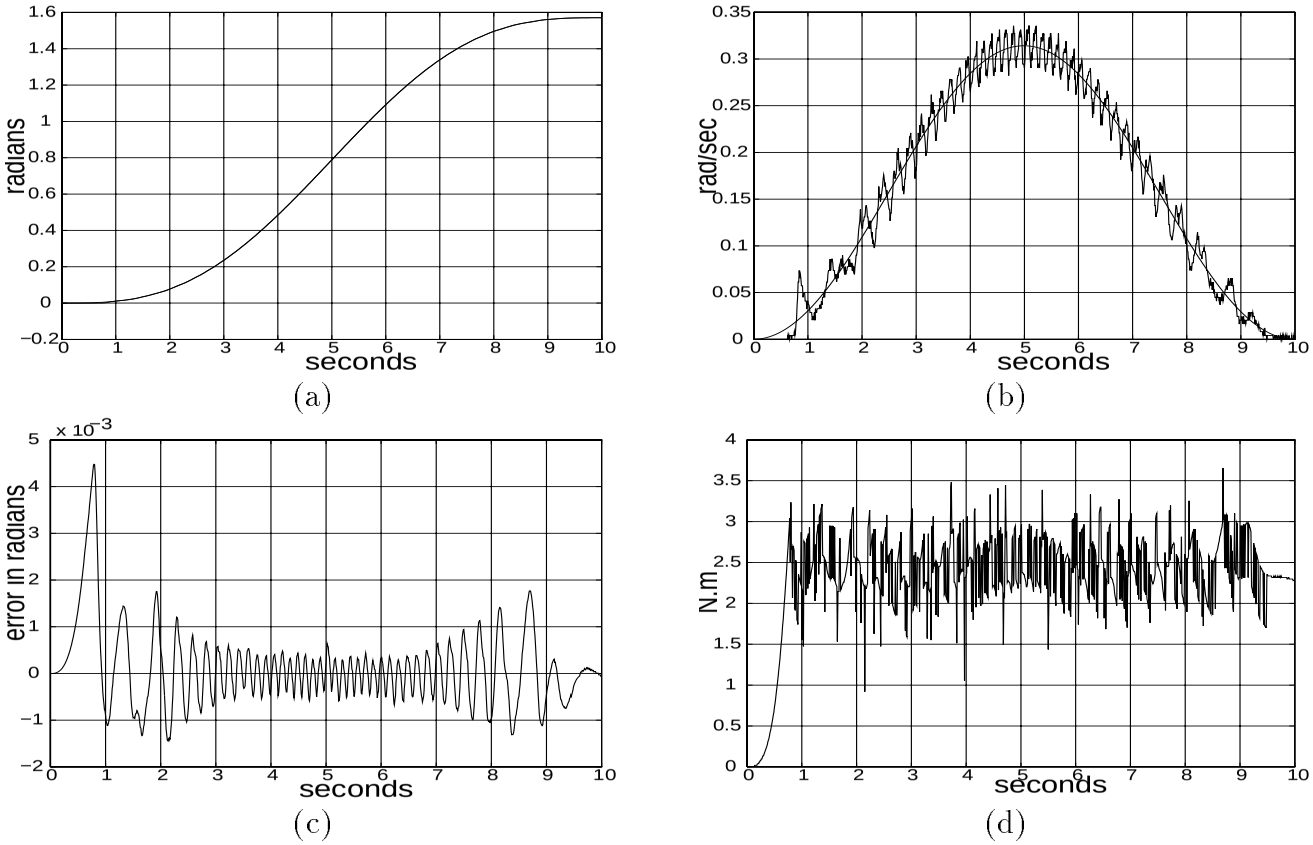

Figure 11: Experimental Results for the PID Controller, Ki=500. (a) Real and commanded position of elbow, (b) Real and commmanded velocity, (c) Tracking error, (d) torque profile

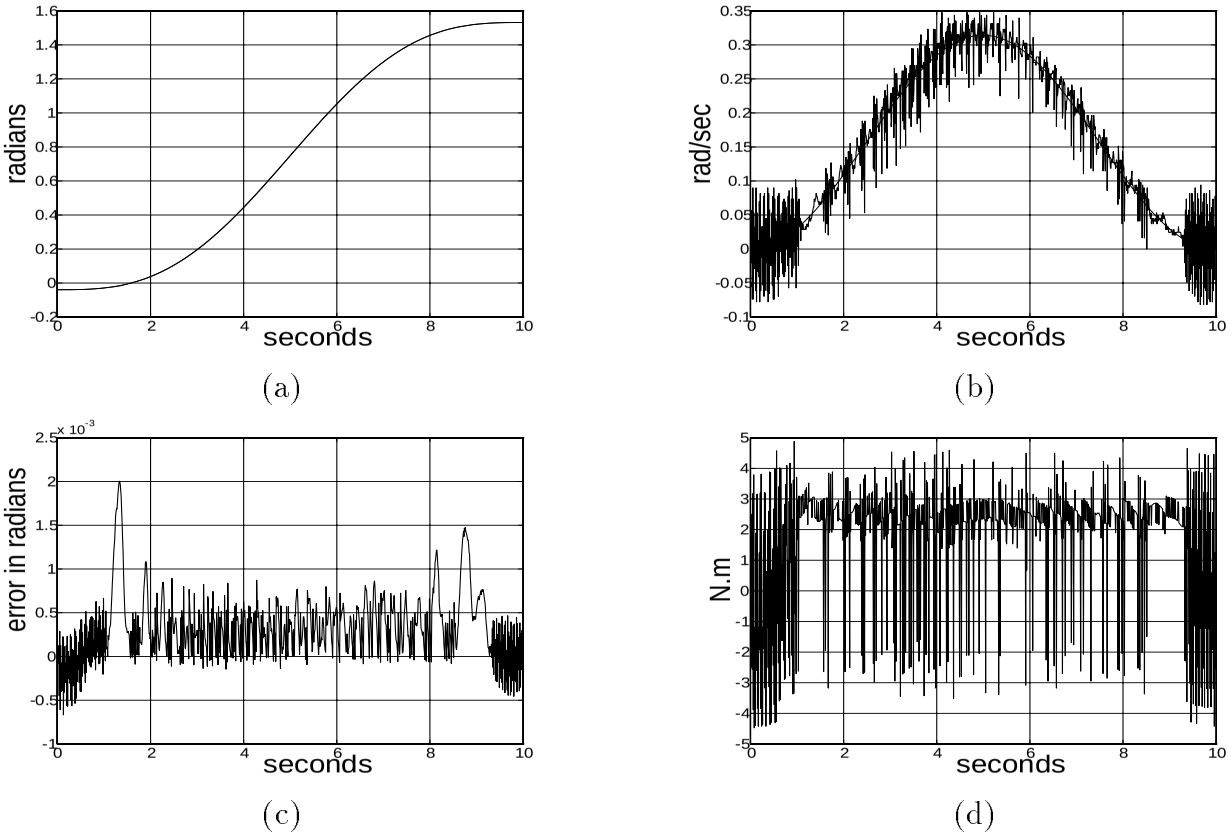

Figure 12: Experimental Results for the Smooth Nonlinear Controller. (a) Real and commanded position of elbow, (b) Real and commmanded velocity, (c) Tracking error, (d) torque profile

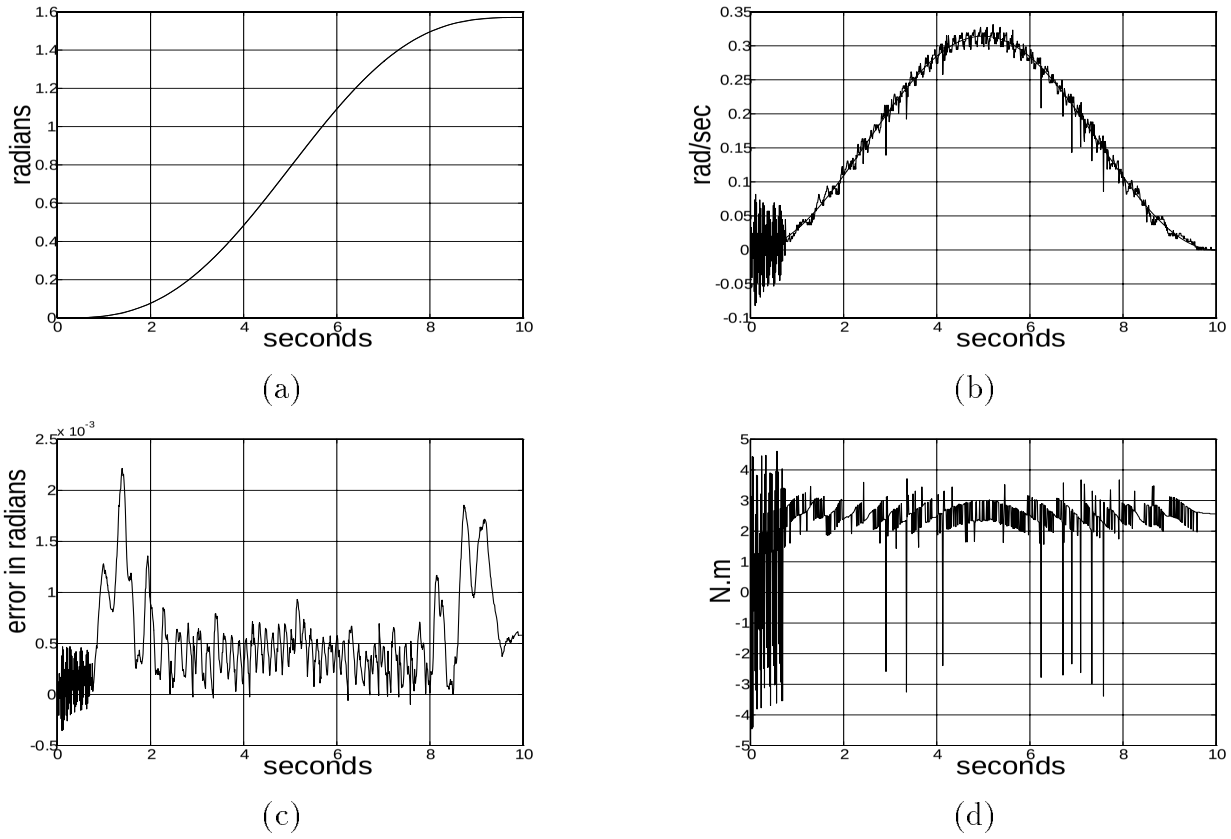

Figure 13: Experimental Results for the Discontinuous Controller. (a) Real and commanded position of elbow, (b) Real and commmanded velocity, (c) Tracking error, (d) torque profile